

Hybrid stochastic and deterministic simulations of calcium blips

S. Rüdiger¹, J.W. Shuai², W. Huisinga³,
Ch. Nagaiah⁴, G. Warnecke⁴, I. Parker², M. Falcke¹

¹Hahn-Meitner Institut, Glienicker Str. 100, 14109 Berlin, Germany

²Department of Neurobiology and Behavior, 1146 McGaugh Hall,
University of California, Irvine, CA 92697, USA

³Department of Mathematics and Computer Science, Arnimallee 6,
14195 Berlin, Germany, and DFG Research Center MATHEON

⁴Institute for Analysis and Numerical Mathematics,
Otto-von-Guericke University Magdeburg,
Universitätsplatz 2, 39106 Magdeburg, Germany

February 27, 2007

Abstract

Intracellular calcium release is a prime example for the role of stochastic effects in cellular systems. Recent models consist of deterministic reaction-diffusion equations coupled to stochastic transitions of calcium channels. The resulting dynamics is of multiple time and spatial scales, which complicates far-reaching computer simulations. In this paper we introduce a novel hybrid scheme that is especially tailored to accurately trace events with essential stochastic variations, while deterministic concentration variables are efficiently and accurately traced at the same time. We use finite elements to efficiently resolve the extreme spatial gradients of concentration variables close to a channel. We describe the algorithmic approach and we demonstrate its efficiency compared to conventional methods. Our single channel model matches experimental data by Mak et al. (PNAS 95 (1998) 15821) and results in intriguing dynamics if calcium is used as charge carrier. Random openings of the channel accumulate in bursts of calcium blips that may be central for the understanding of cellular calcium dynamics.

1 Introduction

Calcium signalling regulates numerous cellular functions as diverse as gene expression, secretion, muscle contraction and synaptic plasticity. A major class of Ca^{2+} signals are triggered by the binding of extracellular ligands to cell surface receptors, resulting in the activation of well known second messenger pathways (6, 12, 30, 32, 44) to evoke Ca^{2+} release from intracellular storage compartments; principally the endoplasmic reticulum (ER) and the sarcoplasmic reticulum. Information is encoded in the spatio-temporal patterning of the resulting increases in cytosolic Ca^{2+} concentration, which may be organized as localized transients (42), propagating waves (11, 18, 33, 37, 47) and global oscillations (6, 9, 48, 63, 64).

Inositol 1,4,5-trisphosphate (IP_3) receptor channels (IP_3R) are present in the ER membrane and regulate the liberation of Ca^{2+} in response to the binding of Ca^{2+} and IP_3 to receptor sites on the channel: that is to say, the open probability of the IP_3R channel depends on the cytosolic calcium concentration as well as the IP_3 concentration (see (43, 45, 59, 61) for reviews). This positive feedback by calcium provides a self-amplifying release mechanism (Calcium Induced Calcium Release; CICR), so that the calcium flux increases nonlinearly with concentrations of IP_3 and Ca^{2+} . In particular, Ca^{2+} released by one channel diffuses in the cytosol and thus increases the open probability of neighboring channels, thereby generating complex spatio-temporal signals.

Experimental observation of local, random release events called puffs indicates that IP_3R channels are grouped into clusters on the ER membrane containing a few tens of channels (10, 14, 41, 46), whose opening is concerted by local diffusion of Ca^{2+} and CICR between adjacent channels. These clusters in turn are randomly distributed across the ER membrane at spacings of a few micrometers. Puffs are now considered to be elemental events of Ca^{2+} signalling (7), underlying global oscillations and waves. They last from 50 to a few hundred milliseconds. Subsequent theoretical studies demonstrated that the observed local calcium elevations are not random due to the small numbers of Ca^{2+} ions, but rather due to the random binding and dissociation of Ca^{2+} and IP_3 at the regulatory binding sites of the IP_3R (see (3, 15, 17–19, 58) and (29) for the ryanodine receptor channel).

It is therefore important for the understanding of calcium signalling, to develop accurate models for stochastic transitions of single channel states. The available experimental data are of two categories: First, there are patch-clamp experiments of single channel currents. Here, IP_3R are inserted into bilayer membranes or are studied in the nuclear membrane and exposed to

fixed concentrations of Ca^{2+} and IP_3 . It is crucial to note that in these experiments a charge carrier different from calcium is used, so that the ions moving through the channel do not bind to receptor sites on the channel and thereby modify the channel gating. Recordings of single channel currents are then analyzed to obtain open probabilities, mean open and mean close times. Several IP_3R models (2, 13, 20, 27, 56, 57) have been developed to describe experimental data obtained from IP_3R reconstituted in bilayer membranes, with the De Young-Keizer model (13) in particular being widely applied. However, there are significant differences in behavior of the reconstituted IP_3R versus that of IP_3R in their native environment of the nuclear envelope (34, 35), and only a few models have incorporated IP_3R data obtained on nuclei membrane (4, 36). On the other hand, the latter models for nuclear receptors are not dynamic models, i.e. they cannot elucidate channel kinetics. Therefore, we have developed a dynamic DeYoung-Keizer-like IP_3R model based on data obtained from patch-clamp of nuclear IP_3R that reproduces experimental findings including the open probability, mean open and closed times (53). The model consists of four identical, independent subunits, each with 13 different states. A channel opens when at least three of its subunits undergo a conformational change to an “active” state after binding IP_3 and Ca^{2+} . For the simulation of blips described in this paper, we simplify this 13-state-subunit IP_3R model to a 9-state-subunit channel model.

A second type of experiment studies IP_3R channels under physiological conditions in intact cells by using fluorescent indicator dyes to monitor Ca^{2+} liberation into the cytosol. The resolution of such imaging techniques is sufficient to detect presumptive single-channel signals (christened “blips”) (41, 42) but it is difficult to study these events in isolation because the opening of one channel usually triggers openings of multiple adjacent channels in the cluster (54). However, because the blips form the fundamental building block from which cellular calcium signals are generated it is important to understand the behavior of IP_3R under physiological conditions where the gating of an individual channel is modulated by the large (> 1000 -fold) changes in local Ca^{2+} concentration that result from Ca^{2+} flux through that channel.

To that end, we simulate stochastic IP_3R channel state dynamics under conditions of no Ca^{2+} feedback (K^+ as the charge carrier), and where Ca^{2+} is the charge carrier. The latter events we refer to as “blips with calcium carrier”. The transitions during a patch-clamp experiment (i.e. no Ca^{2+} feedback) can be simulated by a Markovian scheme with constant transition rates. A standard method (two state Markovian scheme) is to compile a list

of all transitions of the channel in models such as the DYK, and determine a sufficiently small time step dt . The occurrence of each of the stochastic transitions during a specific simulation time step is determined by comparison of a computer random number with the product of the corresponding rate and dt (17, 50). Another, much more efficient method, is the so-called Gillespie algorithm, which determines the time of each transition by using a random number, while a second one is used to determine the next reaction (21). Thus it needs as many steps (and twice as many random numbers) as transitions occurring, which is far less than for the standard method.

While the Gillespie method provides an efficient mean for the study of stochastic channel transitions, the simulation of blips with calcium carrier poses a number of additional problems which we will briefly outline.

(1) The spatio-temporal evolution of free calcium and calcium-binding buffers needs to be simulated simultaneously with that of the channel states. In this work we consider the diffusion and chemical reactions of these species as deterministic processes. In view of the large number of calcium ions and buffer proteins this assumption is a generally accepted strategy (16, 50, 57), which, of course, should be principally proven by simulating the full system stochastically and comparing the results with those from the reduction approach. However, we will not address the validity of that assumption in the current publication.

(2) The spatial extent of a channel is about 10 to 30 nm. Strong currents of calcium lead to very localized calcium concentrations around an open channel. On the other hand, released calcium diffuses rapidly over distances of several micrometers. We thus chose the finite element method to resolve the calcium profile at nanometer scales close to the channel mouth, while utilizing larger and computationally more tractable grid lengths far from the channel.

(3) The time scale of calcium flux upon opening of a channel is of order of microseconds. This time scale cannot be ignored since the binding of calcium to the channel can occur on time scales as short as tens of microseconds. However, simulations need to trace the evolution for many seconds in order to achieve statistically significant estimates of stochastic channel gating. This gap of time scales necessitates an efficient time-stepping method including time adaptivity for both the stochastic and deterministic equations of our model.

(4) The huge and fast concentration changes upon channel openings and closings have a strong impact on the stochastic dynamics of channel binding and unbinding. As mentioned above, the rate of calcium binding may increase by three orders of magnitude upon channel opening owing to the

enormous local calcium concentration increase. This implies that the classical Gillespie algorithm, which rests on the assumption of time independent rates between succeeding stochastic events, cannot be used. Instead, we chose a hybrid method of stochastic and deterministic simulations. This method was described recently for ordinary differential equations (ODEs) coupled to Markov processes (1, 24) and allows for an adaptive step-size integration of the deterministic equations while at the same time accurately tracing the stochastic reaction events.

In this paper we describe the application of the hybrid method introduced by Alfonsi et al. (1) to the calcium system and thus for the first time to a spatially extended system. A second novelty of our approach is the following. The hybrid method assumes that all stochastic events cause a change in the deterministic variables, which is not the case in the Ca^{2+} system. A special feature of the Ca^{2+} system is that the binding/unbinding of Ca^{2+} ions and IP_3 may not change the open/close state of a channel. Therefore, we devised a new hybrid method by combining the adaptive simulation scheme of the deterministic reaction-diffusion dynamics and the simulation technique for stochastic binding/unbinding of Ca^{2+} and IP_3 , which may or may not change the open/close change of the channel. In this paper we describe in detail our hybrid method and, as an example, simulations of calcium blips for a single IP_3R channel. We also compare our hybrid simulation results to results obtained with a method, which uses the Euler scheme for Ca^{2+} diffusion simulation and the two state Markovian approach with sufficiently small time step for the stochastic channel dynamics (50–52), exploiting spherical symmetry properties of a reduced problem. We find good agreement between both methods and conclude that the fastest method for blip simulations would be a hybrid code for stochastic Gillespie transitions coupled to a simulation of a reduced 1D reaction-diffusion equation. Thus we will take full advantage from our 3D finite element/hybrid method in future work on models for Ca^{2+} release from channel clusters, where spherical symmetry cannot be used.

The paper is organized as follows: First, we introduce the basic model of calcium dynamics, which includes the description of all deterministic processes by partial differential equations and the stochastic model of channel state transitions, and discuss the adaptive scheme to solve the deterministic and stochastic equations involving the newly developed hybrid algorithm. We then present results of simulations, first for the purely stochastic model of a single channel with a carrier different from calcium, and then the results for simulations of the full set of equations with calcium as carrier. In the conclusions, we analyze the efficiency and accuracy of the method and

briefly discuss the relevance of our results for present problems in calcium dynamics.

2 Model of calcium dynamics

In the following we will describe each of the components of the model and the equations that we use. As sketched above the model will consist of partial differential equations (PDE) for concentration fields and a Markovian description of discrete stochastic quantities. The concentration fields are the calcium concentration in the cytosol and the buffer concentrations. Stochastic quantities are the discrete states of channel subunits, which determine the open/close state of a channel. The coupling works in the following way: random opening and closing of the channels causes fluctuations of certain source terms in the PDEs, while concentrations enter the transition rates of the Markov processes.

2.1 Partial differential equations for the concentration fields

The calcium concentration is determined by diffusion, the transport of calcium through the ER membrane, and the binding and unbinding of buffer molecules. Here we do not include buffers within the ER. In the cytosol we consider three types of buffers: an exogenous mobile buffer with slow reaction kinetics, a stationary buffer with fast kinetics, and an exogenous dye buffer.

All buffers are assumed to be distributed homogeneously at initial time. Total concentrations of mobile, stationary, and dye buffer are denoted by B_m , B_s , and B_d , the amount of buffer bound to calcium by b_m , b_s , and b_d , respectively. Experimentally, the amounts of exogenously added mobile and dye buffers are controlled. However, the amount of endogenous stationary buffer, comprising contributions from different calcium stores such as mitochondria, is not well characterized.

The buffers are subject to binding and unbinding of calcium, which is

modeled using mass-action kinetics:

$$\begin{aligned}
\frac{\partial c}{\partial t} &= D\nabla^2 c - k_s^+(B_s - b_s)c + k_s^- b_s \\
&\quad - k_m^+(B_m - b_m)c + k_m^- b_m \\
&\quad - k_d^+(B_d - b_d)c + k_d^- b_d, \\
\frac{\partial b_s}{\partial t} &= k_s^+(B_s - b_s)c - k_s^- b_s, \\
\frac{\partial b_m}{\partial t} &= D_m \nabla^2 b_m + k_m^+(B_m - b_m)c - k_m^- b_m, \\
\frac{\partial b_d}{\partial t} &= D_d \nabla^2 b_d + k_d^+(B_d - b_d)c - k_d^- b_d.
\end{aligned} \tag{1}$$

Here, the k_l^\pm ($l = s, m, d$) denote the on and off rates of calcium reacting with the corresponding buffer proteins. The equations are solved in a domain close to an idealized plane membrane patch of $(8 \mu\text{m})^2$ extension. In the direction perpendicular to the membrane we consider a spatial extent of $5 \mu\text{m}$. All boundary conditions except for c at the membrane are no-flux conditions. The remaining boundary condition for c at the ER membrane models the transport through the ER membrane,

$$D\partial_z c = -J, \text{ at } z = 0, \tag{2}$$

and comprises three contributions:

$$J = P_c S(\vec{r}, t)(E - c) - P_p \frac{c^2}{K_d^2 + c^2} + P_l(E - c). \tag{3}$$

Calcium moves from the ER to the cytosol through IP₃ receptors and by a small leak contribution, terms with coefficients P_c and P_l , respectively. In the other direction calcium is resealed into the ER by pumps (P_p). The action of pumps is assumed to be cooperative in calcium and modeled with a quadratic c dependence. K_d is the dissociation constant of the pumps.

The first term in Eq. 3 models the current through the channel. The current in the open state of the channel was found to depend on the cross-membrane difference of the Ca²⁺ concentration (8). For values of the cross-membrane difference in a physiological environment, the current can be approximated by a linear dependence on $(E - c)$, where E denotes the concentration of free Ca²⁺ in the ER. Furthermore, it was found that the current I through a single channel in the open state is about 0.1 pA under physiological conditions, an estimate obtained by analysis of patch-clamp experiments

on single IP₃ channels expressed on membrane bilayers (8) and detailed simulations of the physiological situation (60). This current is modeled by a boundary term, which is constant and non-zero in a specified channel region if the channel is open. Following Thul and Falcke (60) we model the source area of a channel by a circle of radius $R_s = 6$ nm. That radius is an approximation for the radius of the Donnan potential down to which we can assume luminal and cytosolic diffusion properties to hold (39). The corresponding current through this membrane area is derived from

$$I = \pi(6 \text{ nm})^2 P_c (E - c) 2F, \quad (4)$$

where F is the Faraday constant. With a Ca²⁺ concentration in the ER of $E = 700 \mu\text{M}$ and neglecting c , which is close to zero if the channel is closed, we obtain a cross-membrane difference of $700 \mu\text{M}$, resulting in $P_c = 6.32 \times 10^6$ nm/s.

The position of the model channel in the box of coordinates $(0, 8 \mu\text{m}) \times (0, 8 \mu\text{m}) \times (0, 8 \mu\text{m})$ is given by $\vec{X} = (4 \mu\text{m}, 4 \mu\text{m}, 0)$ in the center of the ER membrane. The channel flux term originating from this channel is controlled by the channel state through the factor $S(\vec{r}, t)$, which is defined by:

$$S(\vec{r}, t) = \begin{cases} 1, & \text{if } \|\vec{r} - \vec{X}\| < R_s \text{ and the channel is open,} \\ 0, & \text{otherwise.} \end{cases}$$

2.2 Stochastic model of channel gating

To discuss the dynamics of a single IP₃R we adopt a version of a newly developed stochastic model for the gating of subunits (53) which is based on the DeYoung-Keizer model (13, 28). According to the DeYoung-Keizer model, an IP₃R consists of four identical subunits. There are three binding sites on each subunit: An activating site for Ca²⁺, an inhibiting Ca²⁺ site, and an IP₃ binding site (see Fig. 1). The three binding sites allow for 8 different states X_{ijk} of each subunit. The index i indicates the state of the IP₃ site, j the one of the activating Ca²⁺ site and k the state of the inhibiting Ca²⁺ site. An index is 1 if an ion is bound and 0 if not. Rates of transitions involving binding of a molecule are proportional to the concentration of the respective molecule.

A further transition from X_{110} to a state denoted by X_{ACT} is introduced (53). It represents a conformational change of the subunit related to channel opening within this model. We assume that the channel is open if at least three of the subunits are in the X_{ACT} state.

The binding and dissociation of Ca^{2+} and IP_3 as well as the conformational change are stochastic events rendering the opening and closing of the channel a stochastic process. That stochastic process is coupled to the concentration of cytosolic Ca^{2+} since the binding probabilities per unit time depend on it and vice versa the open/close state of a channel determines the concentration field.

We associate stochastic variables $X_{000}, X_{001}, \dots, X_{ACT}$ to each channel. These variables count the numbers of subunits which are in the respective state, with the sum of all nine variables equal to 4.

Estimation of the calcium concentration on the cytosolic face of the membrane is crucial for comparison with experiments where calcium is used as charge carrier. Due to the strong gradients of calcium around an open channel, the exact position of regulatory Ca^{2+} binding sites may be important for the transition rates in the model. Here, however, we do not study this dependence and simply assume that each of the Ca^{2+} binding processes is determined by the Ca^{2+} concentration in the center of the channel.

3 Numerical method

Our numerical method consists of a coupled solver for the deterministic set of PDEs and the stochastic solver. In view of the multiple scales in length and time we employ an unstructured finite element method and an adaptive linear implicit time-stepping for the deterministic part. The stochastic solver is based on the Gillespie method (21), which is adaptive in the sense that its time step follows the evolution of transition probabilities. A complication arises since the usual Gillespie method solves stochastic processes where the so-called propensities are constant during subsequent transitions (see below). However, for channels with Ca^{2+} as carrier the propensities may change rapidly due to channel openings and closings. This problem is solved by devising the hybrid method described in section 3.2.

3.1 Finite element method for integration of the partial differential equations

We discretized the spatial domain by linear finite elements (tetrahedra). This method is particularly useful when spatial resolution needs to be very high in some regions only. For our simulations of calcium blips we employ a grid with a very fine resolution in the channel area of radius 6 nm. There the grid length is smaller than 1 nm. With increasing distance from the channel the grid is coarsened up to 500 nm. The grid consists of about 30000 points.

Details of the method and the spatial gridding procedure can be found in a forthcoming publication (40).

The finite element discretization results in a coupled set of ODEs, which are solved by a Krylov-W method with 3 stages (49). This method is a linear-implicit Runge-Kutta method of order 2, with an embedded scheme of order 1. Solutions of both orders are used to calculate an approximation of the time-stepping error and to adapt the temporal time step. The arising linear systems are solved by the BiCGSTAB method (62).

The stationary Ca^{2+} concentration gradient around an open channel is shown in Fig. 2. Here we have plotted $[\text{Ca}^{2+}]$ against the distance from the channel center on the membrane and vertical to the membrane. The maximum calcium concentration at the channel is about $112 \mu\text{M}$.

3.2 Hybrid algorithm

The algorithm is based on a recently introduced approach for simulating hybrid models of chemical reaction kinetics in spatially homogeneous systems (1). For the sake of clarity, we introduce our hybrid method for a single channel system—the generalization to multi channel systems will be obvious.

Recall that $X_{000}, X_{001}, \dots, X_{ACT}$ are random variables counting the number of subunits that are in the respective state. The channel changes its state if the occupation of one of the binding sites changes. Such changes are modeled as stochastic events, denoted by R_1, \dots, R_m . The event dynamics is defined in terms of the associated propensity functions $\alpha_1, \dots, \alpha_m$ that characterize the probability per unit time that the corresponding event takes place. The propensities are proportional to the number of subunits X_{su} in the corresponding subunit state of the transition, hence $\alpha_i = X_{su}r_i$, where r_i denotes the transition rate. For instance, denoting the transition from X_{100} to X_{101} by R_1 , we define a propensity $\alpha_1 = X_{100}a_2c$ (see Fig. 1). The product $\alpha_i dt$ is the probability that the event R_i occurs in a given infinitesimal time interval dt .

The Gillespie algorithm allows for simulation of stochastic event systems (21). Given the actual time t , the probability that the next stochastic event occurs in the infinitesimal time interval $[t + \tau, t + \tau + dt]$ and is an R_i event is given by

$$P(\tau, i)dt = \alpha_i \exp(-\alpha_0\tau)dt \quad (5)$$

where $\alpha_0 = \sum_j \alpha_j$ is the sum of all propensities. The probability density $P(\tau, i)$ can be realized by drawing two random numbers r_1 and r_2 from a

uniform distribution in the interval $[0, 1]$, and choosing τ and i such that

$$\alpha_0 \cdot \tau = \ln(1/r_1), \quad \sum_{j=1}^i \alpha_j \leq \alpha_0 \cdot r_2 < \sum_{j=1}^{i+1} \alpha_j. \quad (6)$$

In this way the next event to occur is R_i and it will occur after time τ .

The Gillespie method rests on the assumption that during successive stochastic events the propensities α_i do not change. However, when linking the stochastic channel dynamics to the calcium dynamics, we expect the propensity α_i to change in time due to its dependence on the local calcium concentration c . This effect will be particularly strong for openings and closings of channels, since after such events the local calcium concentration c changes dramatically by three or four orders of magnitude.

To resolve this problem we adopt the recently introduced hybrid method by Alfonsi et al. (1). Within their setting the time τ to the next stochastic event is determined by solving

$$\int_t^{t+\tau} \alpha_0(s, c) ds = \xi, \quad (7)$$

with $\xi = \ln(1/r_1)$, where the sum of propensities α_0 may explicitly depend both on time s and the local calcium concentration. Note that the above equation simplifies to the equation determining τ in (6) in the case of constant α_0 . To determine the time of the next reaction τ , condition (7) is conveniently rewritten in differential form by introducing a variable $g(\tau)$ and solving

$$\dot{g}(s) = \alpha_0(s, c) \quad (8)$$

with initial condition $g(0) = 0$, along with the deterministic equations for c and buffers. A reaction then occurs whenever $g(s)$ reaches the value ξ . As before the specific event R_i is determined based on a second random number r_2 satisfying the second condition in Eq. 6 with propensities evaluated at the event time $t + \tau$.

A special feature of the calcium system is that not all stochastic events change the open/close state of a channel. An event resulting in an opening or closing of the channel occurs only if the number of subunits in the state X_{ACT} changes between 2 and 3 and will be called a *channel transition* in the following. A channel transition has a major impact on the local calcium concentration c , while non-channel transitions do not change the local calcium concentration. Below, the algorithmic realization of our hybrid approach is given. Along the computation of the deterministic part of the

calcium dynamics the stochastic events are traced via Eq. 7 or 8. If a non-channel transition occurs, the stochastic event is performed. The stochastic channel dynamics is updated correspondingly, while there is no influence on the calcium concentration. On the other hand, if a channel transition takes place, both the channel and the calcium dynamics do change. This typically requires a readjustment of the deterministic time step.

The outline of the algorithmic realization is as follows:

1. Initialization

- Set $t_{old} = 0$, $\Delta t > 0$, $c_{old} = c_0$, $X = X_0$, $g_{old} = 0$ and draw a uniform random number r_1 in $[0,1]$ defining $\xi = \ln(1/r_1)$.

2. Deterministic step

- Compute c_{new} and g_{new} based on c_{old} , g_{old} and Δt .
- If the local error criterion (provided by the Krylov-W method) is not met, reduce the step size Δt and go to 2., otherwise define $t_{new} = t_{old} + \Delta t$ and set the new step size Δt according to the time stepping code prediction.

3. If $g_{new} < \xi$ (no stochastic event)

- Set $c_{old} = c_{new}$, $g_{old} = g_{new}$, $t_{old} = t_{new}$, and go to 2.

Else ($g_{new} \geq \xi$, some stochastic event occurs in the time interval $[t_{old}, t_{new}]$)

- Determine the event time $t_s \in [t_{old}, t_{new}]$ by (linear) interpolation, and compute the corresponding calcium concentration c_s at the event time t_s by (linear) interpolation.
- Draw a uniform random number r_2 in $[0,1]$ and determine the stochastic event R_i according to Eq. 6 based on c_s .
- If the next event R_i is not a channel transition
 - Perform the stochastic event R_i to determine the new channel state X .
 - Set $g_{old} = 0$ and recompute g_{new} based on c_s , g_{old} and the remaining time $(t_{new} - t_s)$.
 - Draw a new uniform random number r_1 in $[0,1]$ defining $\xi = \ln(1/r_1)$, and go to 3.

Else (the next event R_i is a channel transition)

- Perform the channel transition R_i to determine the new channel state.
- Set $g_{new} = 0$, and draw a new uniform random number r_1 in $[0, 1]$ defining $\xi = \ln(1/r_1)$
- Set $t_{new} = t_s$, and define new step size $\Delta t = \Delta t_{channel}$ (a sufficiently small number)
- Set $c_{old} = c_s$, and go to 2.

Note that $\Delta t_{channel}$ should be smaller than or similar to the time scale of stochastic transitions after a channel opening/closing, since we linearly interpolate the deterministic solution to determine stochastic transitions between succeeding deterministic time steps. Therefore, fast changes of the deterministic variables after a channel opening/closing need to be approximated numerically at time scales comparable to the stochastic transitions. In our simulations described below $\Delta t_{channel}$ is set to 10^{-5} s.

4 Results for the dynamics of a single channel

4.1 Simulations with fixed calcium concentration

In this section we present results of simulations to test the hybrid method applied to the calcium system. We begin with simulations where the calcium concentration in the cytosol is held fixed to a certain value. Figs. 3 show the open fraction, mean open and mean close time for different calcium concentrations in the cytosol. The connected dots correspond to runs with the hybrid program for 100 s each. The IP_3 level was set to $10 \mu M$ in these simulations. The plot of the open probability (Fig. 3(a)) clearly shows the bell-shaped curve typical for IP_3 receptor channels. Further, one can observe a distinct maximum in the mean open time and a minimum in the mean close time for cytosolic calcium concentrations around $5 \mu M$.

Our model of channel gating was originally obtained by fitting the data of Mak et al. (35). Their results are shown in Fig. 3 by small dots. A detailed description of the parameter estimation by fitting to experimental data can be found in a forthcoming publication (53).

We also compared our results to those from simulations based on a standard Markovian method (53) and found satisfying agreement. This data is shown in Fig. 3 by blue boxes.

4.2 Simulation with calcium as carrier: bursts of blips

We will now present hybrid simulations of our model for a calcium carrying channel. In this situation, the resting free calcium concentration is set to $0.05 \mu\text{M}$, but the opening of the channel and the ensuing calcium current lead to large local cytosolic values of $[\text{Ca}^{2+}]$ of about $110 \mu\text{M}$, thereby vastly increasing the probability of further Ca^{2+} binding.

Fig. 4 shows the evolution of the number of activated subunits for a test run of 35 s. Here the IP_3 concentration was set to $0.1 \mu\text{M}$. During the 35 s interval there are five bursts of channel openings and closings, which are typical for all runs that we have performed. These bursts consist of rapid openings and closings on a ms time scale reflecting the transitions between the states X_{110} and X_{ACT} .

The evolution of a typical burst is shown in Fig. 5 in terms of the number of subunits in the active state X_{ACT} and the Ca^{2+} concentration at the channel mouth. The first opening of the channel after approximately 7.43 s leads to a rapid increase of the local Ca^{2+} concentration, which reaches a stationary value within a few μs . Since activation is a fast process provided that the Ca^{2+} concentration is high, all four subunits are activated within a short time. The switching of subunits between the states X_{110} and X_{ACT} leads then to the repeated openings and closings of the channel.

It is less clear what causes the termination of a burst. We observed that often the termination of a burst is related to inhibition of one subunit, leaving three non-inhibited and activated subunits. The deactivation of one further subunit causes the Ca^{2+} concentration to collapse to values below $1 \mu\text{M}$ within 1 or 2 ms, leaving only residual calcium around the channel, which persists for about 100 ms (see Fig. 5). Consequently the probability for subsequent binding of Ca^{2+} to activating sites is small, which can lead to a prolonged closure of the channel.

We have made a series of simulations to determine the open fraction, mean open time, and mean close time for different IP_3 concentrations. The open fraction is shown in Fig. 6(a). It increases with increased levels of $[\text{IP}_3]$. The values are always far from the maximum 80% found for channels without Ca^{2+} carrier (compare Fig. 3).

Figs. 6(b) and (c) show the estimated mean open and mean close times for different IP_3 concentrations. The mean open time depends significantly on the IP_3 concentration and increases from about 5 to 8 ms. The mean close time reaches values of 180 ms for small IP_3 concentration and lowers to about 40 ms for larger IP_3 concentration.

We have again compared the results of our simulations using the hybrid

method with results of the two state Markovian method (53). To calculate the cytosolic Ca^{2+} concentration we exploited spherical symmetry to simplify the Laplace operator according to the numerical scheme introduced by Smith et al. (55). The spatial grid distance used in these simulations was $dx = 15$ nm. Results of these simulations, supporting the data obtained by the hybrid method, are shown in Fig. 6 by blue boxes.

Inspection of time series showed that the duration of bursts depends on the IP_3 concentration. For small concentration values, below those of the example shown in Fig. 4, we find typical burst durations of 300 ms and less. This behavior is presumably related to the binding of IP_3 to less than four subunits if the IP_3 concentration is low. Then the chance for the termination of a series of blips is much higher than with all four subunits available for activation.

5 Conclusions

In this paper we have described the first computational approach to intracellular calcium dynamics, which takes into account the coupling of stochastic and deterministic evolution equations in an accurate and efficient way. The strong localization of Ca^{2+} ions around an open channel necessitates the use of finite elements. This method has also been successfully used by other groups (23, 26, 38). Here we concentrated on the additional problem of fast temporal scales, which arise from the channel gating and local relaxation of calcium concentrations. The hybrid algorithm to reliably link the stochastic transitions to deterministic concentration variables was described in detail. The hybrid method is an extension of the exact Gillespie method for chemical master equations, and is in general used to speed up the update of species with large quantities. We have adapted the hybrid method of Alfonsi et al. (1) to solve DYK-type transition schemes where only a few of the transitions lead to direct changes in deterministic concentrations. Furthermore, to our knowledge we have used the hybrid method for the first time in conjunction with reaction-diffusion equations, that is, in systems, where the concentration variables exhibit spatial dependence. The results of extensive simulations were compared with results of a standard two state method. This method gives accurate results for sufficiently small time steps. Using a time step of 10^{-5} s for the two state method a satisfactory agreement of both methods was found.

The advantage of the hybrid method is a much larger typical time step and a reduced number of required random numbers. For a run of 35 s as

shown in Fig. 4 the two state Markovian method needs 3.5 million steps and 3.5 million random numbers. The hybrid simulation required about 36400 steps of the deterministic solver for the same run, where most of the steps are required for output at every ms, and two random numbers per transition, i.e., around 12000 random numbers (for the run shown in Fig. 4 we found around 6000 stochastic transitions.)

We note that within the current problem of single channel simulations a one-dimensional spatial discretization of a spherically symmetric channel can be used, as was done in our simulations using the two state method. This approach has the advantage of speeding up the deterministic simulation step considerably compared to the fully three-dimensional simulations used with the hybrid code. Therefore we found that the total simulation times using the hybrid code were higher than for the two state method based on the 1D model exploiting spherical symmetry. However, the ultimate goal of our research is the simulation of one or several clusters of channels. We plan to simulate the release of calcium from about 20 to 60 channels per cluster, which are located on a plane membrane patch. Here spherical symmetry cannot be used and the full advantage of hybrid modeling is apparent.

A possible improvement of our simulation technique regards the time step for the deterministic equation. Here we use an implicit solver, which allows large time steps even if fast relaxation processes occur. However, we need to accurately trace the evolution of propensities and thus of the Ca^{2+} concentration and cannot, in the current computer code, take advantage of large time steps. The use of time stepping techniques with dense output may mitigate this problem (22). Such methods allow large time steps but provide the solution at intermediate times with much higher accuracy than the linear interpolation that we are using in the current code.

We want to stress that the hybrid method can be generalized for use in models of many different biochemical systems. Fast time scales and the existence of processes with large and small numbers of molecules often prohibit efficient simulation of the complete chemical master equation. The solution that we propose is the simulation of ODEs or PDEs coupled to stochastic molecular processes, which are expected to introduce fluctuations. We have shown in this paper that the coupling of both systems can be efficiently performed with the hybrid method.

We are aware of the fact that the new method in principal needs to be validated solving both the channel as well as the calcium and the buffer dynamics fully stochastically according to the reaction diffusion master equation (5, 25, 31). Due to the large amount of calcium and buffer molecules in the system, this would not even be feasible on supercomputers, since the

computational efforts scales with the number of reactions (including diffusion as a first order (pseudo) reaction, see e.g. (25)). However, pursuing along a similar line as in (1), we may justify our new approach. Since calcium and dye buffer concentrations are high, as are the diffusion and binding rate constants for calcium-dye binding processes, the resulting propensities will be large. As a consequence, all diffusion reactions as well as the calcium dye binding processes can be approximately modelled deterministically. However, the propensities corresponding to the channel dynamics will be small to moderate, since the associated rate constants are small. This finally results in the herein presented model, a deterministic reaction-diffusion model for calcium and the dye buffer, coupled to a stochastic model of the channel kinetics. The proposed algorithmic realization is therefore based on the same theoretical justification as is the method in Alfonsi et al. (1).

We finally discuss the relevance of our work for the understanding of calcium dynamics. First of all, our model uses an additional active state compared to the DYK model. This additional state enables us to fit short mean open and mean close times, which were found in experimental data and which could not be fitted using the DYK model. Furthermore, we found that the existence of the additional conformational change results in bursts of rapid openings and closings if calcium is used as a carrier, similar to what was found by Swillens et al. (57). In this and in further respects the 9-state model for subunit dynamics will be a better model for ongoing studies of calcium dynamics. For instance, the existence of two time scales of activity inherent to the 9-state model (i.e., the mean open time and the duration of a burst) may well have consequences for the dynamics of clusters of channels and will be studied in more detail in the future.

6 Acknowledgment

S.R. and C.N. are supported by grants FA 350/6-1 and WA 633/16-1 of the Deutsche Forschungsgemeinschaft within the priority program SPP 1095 “Analysis, Modeling, and Simulation of Multiscale Problems”. W.H. acknowledges financial support by the DFG Research Center MATHEON “Mathematics for key technologies: Modelling, simulation, and optimization of real-world processes”. I.P. acknowledges support from NIH grants (GM48071 and GM65830).

7 Appendix

In Table 1 we provide the complete list of parameters of our model.

References

1. Alfonsi, A., E. Cances, G. Turinici, B. D. Ventura, and W. Huisinga. 2005. Exact simulation of hybrid stochastic and deterministic models for biochemical systems. *ESAIM: Proc.* 14:1–13.
2. Atri, A., J. Amundson, D. Clapham, and J. Sneyd. 1993. A single pool model for intracellular calcium oscillations and waves in the *Xenopus laevis* oocyte. *Biophys.J.* 65:1727–1739.
3. Bär, M., M. Falcke, L. Tsimring, and H. Levine. 2000. Discrete stochastic modeling of calcium channel dynamics. *Phys.Rev.Lett.* 84:5664–5667.
4. Baran, I. 2003. Integrated luminal and cytosolic aspects of the calcium release control. *Biophys.J.* 84:1470–1485.
5. Baras, F., and M. M. Mansour. 1997. Microscopic simulation of chemical instabilities. *Adv. Chem. Phys.* 100:393–475.
6. Berridge, M. 1990. Calcium oscillations. *J.Biol.Chem.* 265:9583–9586.
7. Berridge, M., and B. Potter. 1990. Inositol trisphosphate analogues induce different oscillatory patterns in *Xenopus* oocytes. *Cell.Regul.* 1:675–681.
8. Bezprozvanny, I., and B. Ehrlich. 1994. Inositol(1,4,5)-trisphosphate $\text{Ins}(1,4,5)\text{P}_3$ -gated channels from cerebellum: conduction properties for divalent cations and regulation by intraluminal calcium. *J.Gen.Physiol.* 104:821–856.
9. Bird, G., M. Rossier, J. Obie, and J. P. J.W. 1993. Sinusoidal oscillations in intracellular calcium due to negative feedback by protein kinase C. *J.Biol.Chem.* 268:8425–8428.
10. Bootman, M., E. Niggli, M. Berridge, and P. Lipp. 1997. Imaging the hierarchical Ca^{2+} signalling in HeLa cells. *J.Physiol.* 499:307–314.
11. Camacho, P., and J. Lechleiter. 1993. Increased frequency of calcium waves in *Xenopus laevis* oocytes that express a calcium-atpase. *Science.* 260:226–229.

12. Capiod, T., J. Noel, L. Combettes, and M. Claret. 1991. Cyclic AMP-evoked oscillations of intracellular $[Ca^{2+}]$ in guinea-pig hepatocytes. *Biochem.J.* 275:277–280.
13. DeYoung, G., and J. Keizer. 1992. A single-pool inositol 1,4,5-trisphosphate-receptor-based model for agonist-stimulated oscillations in Ca^{2+} concentration. *Proc.Natl.Acad.Sci USA.* 89:9895–9899.
14. Dupont, G., S. Swillens, C. Clair, T. Tordjmann, and L. Combettes. 2000. Hierarchical organization of calcium signals in hepatocytes: from experiments to models. *Biochim.Biophys.Acta.* 1498:134–152.
15. Falcke, M. 2003. Buffers and oscillations in intracellular Ca^{2+} dynamics. *Biophys.J.* 84:28–41.
16. Falcke, M. 2003. Deterministic and stochastic models of intracellular Ca^{2+} waves. *New Journal of Physics.* 5:96.1–96.28.
17. Falcke, M. 2003. On the role of stochastic channel behavior in intracellular Ca^{2+} dynamics. *Biophys.J.* 84:42–56.
18. Falcke, M. 2004. Reading the patterns in living cells - the Physics of Ca^{2+} signaling. *Advances in Physics.* 53:255–440.
19. Falcke, M., L. Tsimring, and H. Levine. 2000. Stochastic spreading of intracellular Ca^{2+} release. *Phys.Rev.E.* 62:2636–2643.
20. Freiman, D., and S. P. Dawson. 2004. A model of the ip3 receptor with a luminal calcium binding site: stochastic simulations and analysis. *Cell Calcium.* 35:403–413.
21. Gillespie, D. T. 1977. Exact stochastic simulation of coupled chemical reactions. *J. Phys. Chem.* 8:2340.
22. Hairer, E., and G. Wanner. 1996. Solving ordinary differential equations: Stiff and differential-algebraic problems. Springer.
23. Hanhart, A. L., M. K. Gobbert, and L. T. Izu. 2004. A memory-efficient finite element method for systems of reaction-diffusion equations with non-smooth forcing. *J. Comp. Appl. Math.* 169:431–458.
24. Haseltine, E. L., and J. B. Rawlings. 2002. Approximate simulation of coupled fast and slow reactions for stochastic chemical kinetics. *J. Chem. Phys.* 117:6959.

25. Hattne, J., D. Fange, and J. Elf. 2005. Stochastic reaction-diffusion simulation with mesord. *Bioinformatics*. 21:2923–2924.
26. Izu, L. T., S. A. Means, J. N. Shadid, Y. Chen-Izu, and C. W. Balke. 2006. Interplay of ryanodine receptor distribution and calcium dynamics. *Biophys. J.* 91:95–112.
27. Kaftan, E., B. Ehrlich, and J. Watras. 1997. Inositol 1,4,5-trisphosphate (InsP₃) and calcium interact to increase the dynamic range of InsP₃ receptor-dependent calcium signaling. *J.Gen.Physiol.* 110:529–538.
28. Keizer, J., and G. DeYoung. 1994. Simplification of a realistic model of IP₃-induced Ca²⁺ oscillations. *J.theor.Biol.* 166:431–442.
29. Keizer, J., and G. Smith. 1998. Spark-to-wave transition: saltatory transmission of calcium waves in cardiac myocytes. *Biophys.Chem.* 72:87–100.
30. Kummer, U., L. Olsen, C. Dixon, A. Green, E. Bornberg-Bauer, and G. Baier. 2000. Switching from simple to complex oscillations in calcium signaling. *Biophys.J.* 79:1188–1195.
31. Kuramoto, Y. 1974. Effects of diffusion on the fluctuations in open systems. *Prog. Theor. Phys.* 52:711–713.
32. LeBeau, A., D. Yule, G. Groblewski, and J. Sneyd. 1999. Agonist-dependent phosphorylation of the inositol 1,4,5-trisphosphate receptor - a possible mechanism for agonist-specific calcium oscillations in pancreatic acinar cells. *J.Gen.Physiol.* 113:851–871.
33. Lechleiter, J., S.Girard, E.Peralta, and D.Clapham. 1991. Spiral calcium wave propagation and annihilation in *Xenopus laevis* oocytes. *Science*. 252:123–126.
34. Mak, D., and J. Foskett. 1997. Single-channel kinetics, inactivation, and spatial distribution of inositol trisphosphate (IP₃) receptor in *Xenopus* oocyte nucleus. *J.Gen.Physiol.* 109:571–587.
35. Mak, D., S. McBride, and J. Foskett. 1998. Inositol 1,4,5-tris-phosphate activation of inositol tris-phosphate receptor Ca²⁺ channel by ligand tuning of Ca²⁺ inhibition. *Proc.Nat.Acad.Sci.USA*. 95:15821–15825.
36. Mak, D., S. McBride, and J. Foskett. 2003. Spontaneous channel activity of the inositol 1,4,5-trisphosphate (InsP₃) receptor (InsP₃R). application

- of allosteric modeling to calcium and InsP_3 regulation of the InsP_3R single-channel gating. *J.Gen.Physiol.* 122:583–603.
37. Marchant, J., and I. Parker. 2001. Role of elementary Ca^{2+} puffs in generating repetitive Ca^{2+} oscillations. *The EMBO Journal.* 20:65–76.
 38. Means, S., A. J. Smith, J. Shepherd, J. Shadid, J. Fowler, R. J. H. Wojcikiewicz, T. Mazel, G. D. Smith, and B. S. Wilson. 2006. Reaction diffusion modeling of calcium dynamics with realistic er geometry. *Biophys. J.* 91:537–557.
 39. Mejia-Alvarez, R., C. Kettlun, E. Rios, and M. Stern. 1999. Unitary calcium current through cardiac ryanodine receptors under physiological conditions. *J.Gen.Physiol.* 113:177–186.
 40. Nagaiah, C., S. Rüdiger, M. Falcke, and G. Warnecke. 2006. *in prep.* .
 41. Parker, I., J. Choi, and Y. Yao. 1996. Elementary events of InsP_3 -induced Ca^{2+} liberation in *Xenopus* oocytes: hot spots, puffs and blips. *Cell Calcium.* 20:105–121.
 42. Parker, I., and Y. Yao. 1996. Ca^{2+} transients associated with openings of inositol trisphosphate gated channels in *Xenopus* oocytes. *J.Physiol.(Lond.)*. 491:663–668.
 43. Patel, S., S. Joseph, and A. Thomas. 1999. Molecular properties of inositol 1,4,5-trisphosphate receptors. *Cell Calcium.* 25:247–264.
 44. Peterson, C., E.C.Toescu, and O. Petersen. 1991. Different patterns of receptor activated cytoplasmic Ca^{2+} oscillations in single pancreatic acinar cells: dependence on receptor type, agonist concentration and intracellular Ca^{2+} buffering. *The EMBO J.* 10:527–533.
 45. Putney, J., and G. Bird. 1993. The inositolphosphate-calcium signaling system in nonexcitable cells. *Endocrine Reviews.* 14:610–631.
 46. Reber, B., and B. Schindelholz. 1996. Detection of a trigger zone of bradykinin-induced fast calcium waves in PC12 neurites. *Pflügers Arch.-Eur.J.Physiol.* 432:893–903.
 47. Ridgway, E., J. Gilkey, and L. Jaffe. 1977. Free calcium increases explosively in activating medaka eggs. *Proc.Natl.Acad.Sci. USA.* 74:623–627.

48. Rooney, T., E. Sass, and A. Thomas. 1989. Characterization of cytosolic calcium oscillations induced by phenylephrine and vasopressin in single fura-2-loaded hepatocytes. *J.Biol.Chem.* 264:17131–17141.
49. Schmitt, B. A., and R. Weiner. 1995. Matrix-free w-methods using a multiple Arnoldi iteration. *Appl. Num. Math.* 18:307–320.
50. Shuai, J., and P. Jung. 2002. Stochastic properties of Ca^{2+} release of inositol 1,4,5-trisphosphate receptor clusters. *Biophys.J.* 83:87–97.
51. Shuai, J., and P. Jung. 2003. Optimal ion channel clustering for intracellular calcium signaling. *Proc.Nat.Acad.Sci.USA.* 100:506–510.
52. Shuai, J., and I. Parker. 2005. Optical single-channel recording by imaging Ca^{2+} flux through individual ion channels: theoretical considerations and limits to resolution. *Cell Calcium.* 37:283–299.
53. Shuai, J., J. E. Pearson, and I. Parker. 2006. *in prep.* .
54. Shuai, J., H. J. Rose, and I. Parker. 2006. The number and spatial distribution of IP_3 receptors underlying calcium puffs in xenopus oocytes. *acc. by Biophys. J. (BIOFAST Sep 15 2006).* .
55. Smith, G., J. Wagner, and J. Keizer. 1996. Validity of the rapid buffer approximation near a point source of calcium ions. *Biophys.J.* 70:2527–2539.
56. Sneyd, J., and J.-F. Dufour. 2002. A dynamic model of the type-2 inositol trisphosphate receptor. *Proc.Nat.Ac.Sci. USA.* 99:2398–2403.
57. Swillens, S., P. Champeil, L. Combettes, and G. Dupont. 1998. Stochastic simulation of a single inositol 1,4,5-trisphosphate-sensitive Ca^{2+} channel reveals repetitive openings during blip-like Ca^{2+} transients. *Cell Calcium.* 23:291–302.
58. Swillens, S., G. Dupont, and P. Champeil. 1999. From calcium blips to calcium puffs: Theoretical analysis of the requirements for interchannel communication. *Proc.Nat.Acad.Sci.USA.* 96:13750–13755.
59. Taylor, C. 1998. Inositol trisphosphate receptors: Ca^{2+} -modulated intracellular Ca^{2+} channels. *Biochimica and Biophysica Acta.* 1436:19–33.
60. Thul, R., and M. Falcke. 2004. Release currents of IP_3 receptor channel clusters and concentration profiles. *Biophys.J.* 86:2660–2673.

61. Tsien, R., and R. Tsien. 1990. Calcium channels, stores and oscillations. *Annu.Rev.Cell Biol.* 6:715–760.
62. van der Vorst, H. A. 1994. Bi-CGSTAB: A fast and smoothly converging variant of bi-cg for the solution of nonsymmetric linear systems. *SIAM J. Sci. Stat. Comput.* 13:631–644.
63. Woods, N., K. Cuthbertson, and P. Cobbold. 1986. Repetitive transient rises in cytoplasmic free calcium in hormone-stimulated hepatocytes. *Nature.* 319:600–602.
64. Zimmermann, B. 2000. Control of InsP₃-induced Ca²⁺ oscillations in permeabilized blowfly salivary gland cells: contribution of mitochondria. *J.Physiol.* 525:707–719.

Parameter	Value	Unit
channel flux coefficient P	6.32×10^6	nm s^{-1}
single channel radius R_s	6	nm
pump flux coefficient P_p	40000	$\text{nm } \mu\text{M s}^{-1}$
pump dissociation coefficient K_d	0.2	μM
Ca^{2+} concentration in ER, E	700	μM
Ca^{2+} concentration in cytosol at rest, c_0	0.05	μM
leak flux coefficient $P_l = P_p c_0^2 / E(c_0^2 + K_d^2)$	3.36	nm s^{-1}
diffusion coefficient D of free cytosolic Ca^{2+}	200	$\mu\text{m}^2 \text{s}^{-1}$
diffusion coefficient D_m of mobile buffer	200	$\mu\text{m}^2 \text{s}^{-1}$
diffusion coefficient D_{dye} of dye buffer	15.0	$\mu\text{m}^2 \text{s}^{-1}$
on-rates of fast buffers:		
k_s^+	50	$(\mu\text{M s})^{-1}$
k_m^+	5	$(\mu\text{M s})^{-1}$
k_{dye}^+	150	$(\mu\text{M s})^{-1}$
dissociation constants of buffers $K_i = k_i^- / k_i^+$:		
K_s	2	μM
K_m	0.15	μM
K_{dye}	2	μM
total concentrations of buffers:		
B_s	80	μM
B_m	300	μM
B_{dye}	40	μM
subunit kinetics, note $b_i = a_i d_i$		
IP ₃ binding		
a_1, a_3	80	$(\mu\text{M s})^{-1}$
d_1	0.008	μM
d_3	0.5	μM
inhibiting, with IP ₃		
a_2	0.04	$(\mu\text{M s})^{-1}$
d_2	12	μM
inhibiting, without IP ₃		
a_4	0.4	$(\mu\text{M s})^{-1}$
d_4	0.192	μM
activating		
a_5	15	$(\mu\text{M s})^{-1}$
d_5	0.8	μM
open conformational transition		
a_0	550	μM
b_0	80	μM

Table 1:

Figure Legends

Figure 1.

The stochastic model of channel gating is given by 26 possible transitions of each of the four subunits. p and c denote the concentrations of IP_3 and Ca^{2+} , respectively.

Figure 2.

The stationary Ca^{2+} concentration for an open channel directly at the ER membrane (solid) and perpendicular to the membrane (dashed) as calculated with the finite element discretization.

Figure 3.

Open fraction (a), mean open (b) and mean close time (c) versus cytosolic $[\text{Ca}^{2+}]$ for $[\text{IP}_3] = 10 \mu\text{M}$. Connected large dots: hybrid simulations for runs of 100 s, small dots: data from experimental work of Mak et al. (35), blue boxes: two state Markovian method for runs of 10^5 s.

Figure 4.

The evolution of the number of subunits in state X_{ACT} for a simulation run with $[\text{IP}_3]=0.1 \mu\text{M}$. The channel is open if $X_{ACT} = 3$ or 4. The resting concentration of Ca^{2+} was $0.05 \mu\text{M}$.

Figure 5.

The Ca^{2+} concentration at the channel mouth and the number of subunits in the active state, X_{ACT} , during the second burst shown in Fig. 4. After the last closing of the burst residual Ca^{2+} decays in about 100 ms.

Figure 6.

Open fraction (a), mean open duration (b), and mean close duration (c) versus IP_3 concentration using calcium carrier. Circles - hybrid simulations (simulation time: 200 s), boxes - simulation with two state Markovian method (150 s).

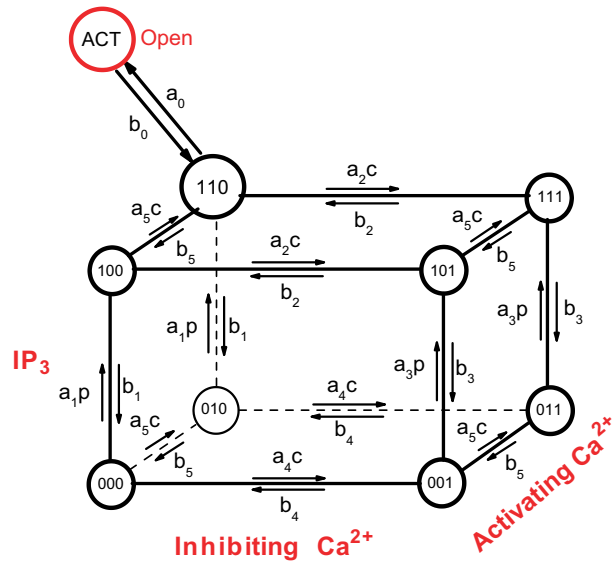


Figure 1:

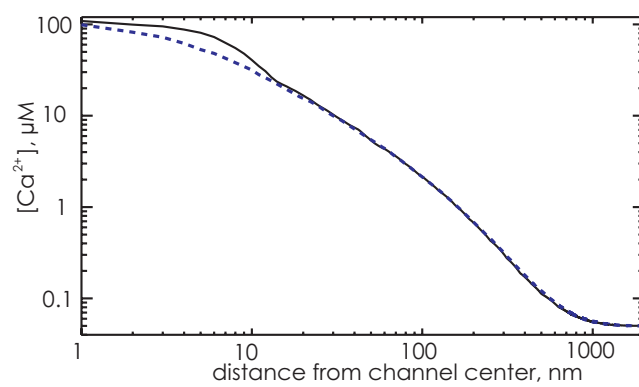


Figure 2:

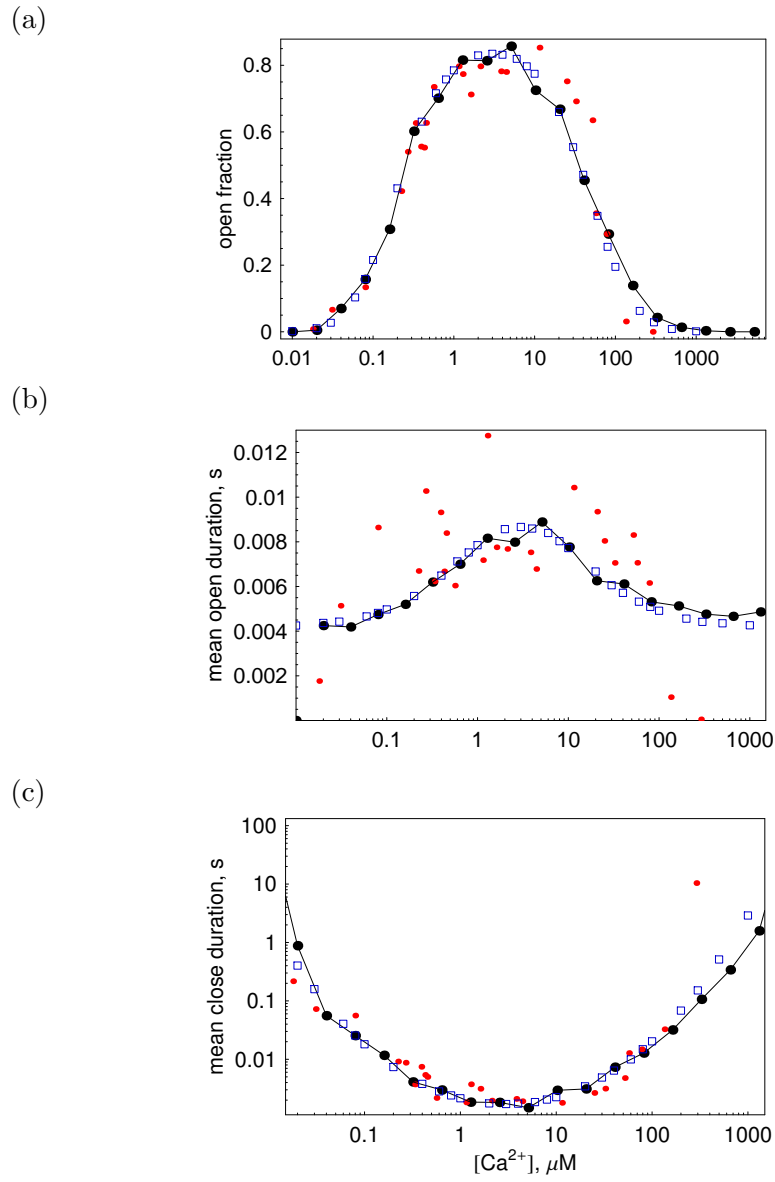


Figure 3:

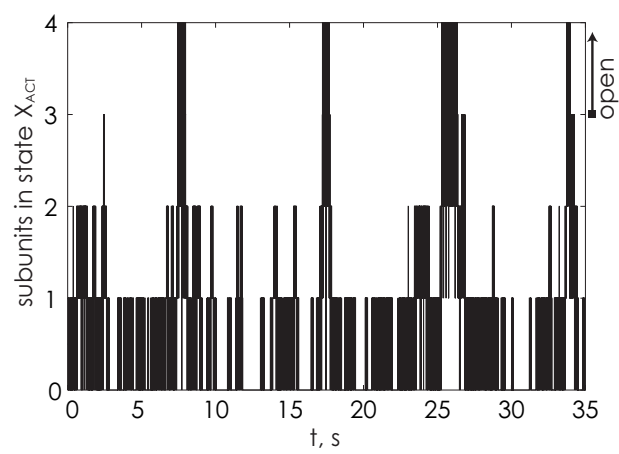


Figure 4:

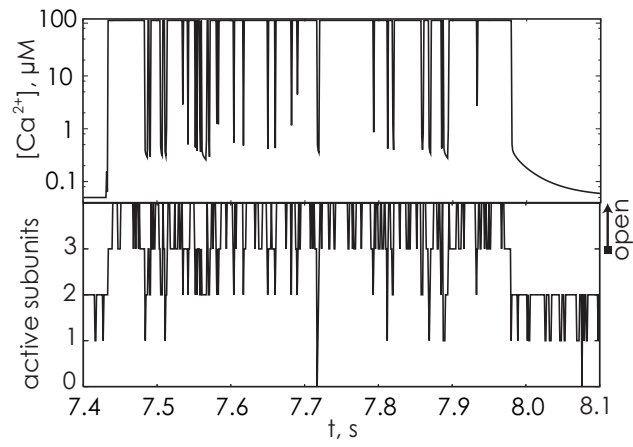
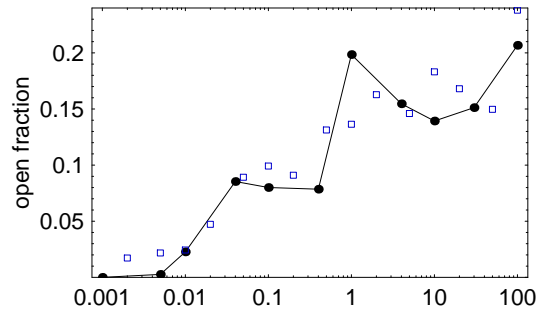
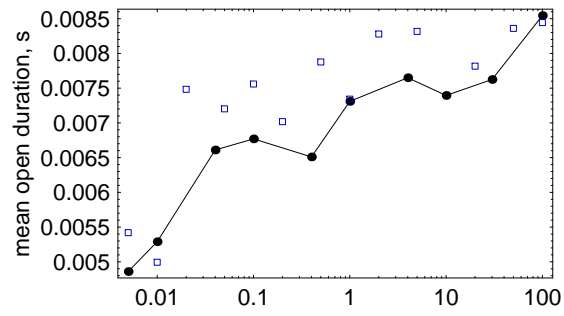


Figure 5:

(a)



(b)



(c)

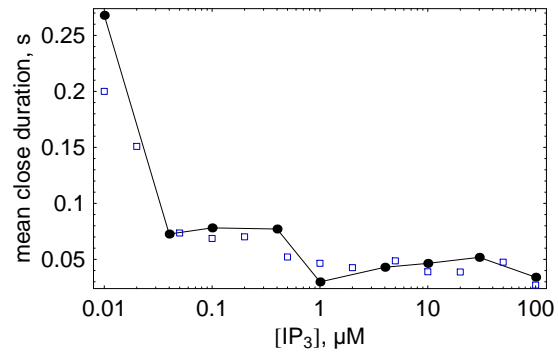


Figure 6: